

CrossFusion: Interleaving Cross-modal Complementation for Noise-resistant 3D Object Detection

Yang Yang
Zhejiang University of Technology
yangyang98@zjut.edu.cn

Weijie Ma
The Chinese University of Hong Kong(Shenzhen)
weijiema@link.cuhk.edu.cn

Hao Chen
Zhejiang University
haochen.cad@zju.edu.cn

Linlin Ou
Zhejiang University of Technology
linlinou@zjut.edu.cn

Xinyi Yu
Zhejiang University of Technology
yuxy@zjut.edu.cn

Abstract

The combination of LiDAR and camera modalities is proven to be necessary and typical for 3D object detection according to recent studies. Existing fusion strategies tend to overly rely on the LiDAR modal in essence, which exploits the abundant semantics from the camera sensor insufficiently. However, existing methods cannot rely on information from other modalities because the corruption of LiDAR features results in a large domain gap. Following this, we propose CrossFusion, a more robust and noise-resistant scheme that makes full use of the camera and LiDAR features with the designed cross-modal complementation strategy. Extensive experiments we conducted show that our method not only outperforms the state-of-the-art methods under the setting without introducing an extra depth estimation network but also demonstrates our model’s noise resistance without re-training for the specific malfunction scenarios by increasing 5.2% mAP and 2.4% NDS.

1. Introduction

3D object detection plays a crucial role in autonomous driving, and the quality of the detection can directly determine the safety level in practical application scenarios. Thanks to the accurate 3D information of LiDAR, some previous works [7, 39, 45] have achieved satisfactory results on the nuScenes dataset [3]. Recently, some LiDAR-Camera fusion methods [1, 5, 6, 13] have shown more powerful perception capabilities based on the strong geometric prior knowledge of the point cloud. However, in au-

tonomous driving scenarios, where LiDAR signals are often affected by weather, light, reflections, etc. The performance of these methods is not ideal. Due to design limitations, image information cannot amend in this situation as expected.

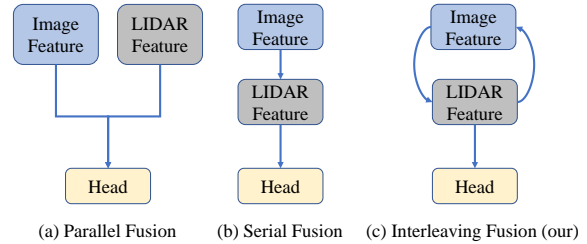


Figure 1. Comparison of LiDAR-camera fusion strategies. (a) Parallel fusion: Each branch can work independently, but the 2D-3D projection process is complex. (b) Serial Fusion: Overly rely on the LiDAR. (c) Our method: Complementary modal information through modal interleaving.

As shown in Fig. 1, the existing fusion models can be mainly divided into two forms, parallel fusion and serial fusion. Parallel fusion maps image features and point cloud features into a unified space and uses the fusion features to locate the object [6, 15, 17]. The serial fusion, people usually use the image features from specified regions to enhance the point cloud information results [30, 31, 38], or inject image features and point cloud features into proposal [1, 5, 13].

Although these methods have achieved impressive results, they still have shortcomings. The serial fusion method has two potential problems. Firstly, their performance is inherently dependent on the precise 3D information provided by LiDAR, but they do not deeply explore the importance

of images for localization. If low-quality LiDAR features are input, they may produce inaccurate results. This situation could pose a safety hazard to autonomous driving decisions. Secondly, they do not seem to adequately consider the information interaction between LiDAR and images, which may hinder the complementary properties between the modalities. Therefore, the association between geometric and depth information specific to sparse point cloud features and dense semantic features of images may be limited.

We believe that the LiDAR-camera fusion framework’s core challenge lies in exploiting complementarity. In other words, when the features provided by one sensor are contaminated, the fusion model can adaptively invoke features from the other modality to resist the perturbation of the noise and balance the weight of the two modalities.

In this paper, we design a framework for modal interleaving fusion, dubbed CrossFusion(see Fig. 2). Specifically, we design a two-stage network. First, we generate a set of proposal bounding boxes by LiDAR features, and then we enhance query features with points inside the proposal to force it to explore features of difficult samples. Next, we use cross decoder to alternately fuse image features and LiDAR features to adaptively build up the modal complementation capability to obtain better robustness. On the basis of the LiDAR decoder, we extract image features from the image feature encoder to alleviate the domain gap between the two modalities. Our contributions are summarized as follows:

- We propose a novel LiDAR-camera fusion model for 3D target detection. It achieves modal complementarity through an interleaving fusion architecture. It also exhibits excellent robustness against various LiDAR information quality degradations without re-training.
- We introduce a pluggable feature enhancement operation to the proposal query, which encourages the network to learn hard samples and balances the contribution of image features and LiDAR features to perception.
- We achieve state-of-the-art methods under the setting without introducing an extra depth estimation network.

2. Related Works

Below are two main categories of 3D detection methods based on the amount and type of modality.

Single-sensor. There are two main types of single-sensor 3D detection, which are LiDAR-only and camera-only. Point clouds are extensively used in 3D detection as a fundamental and effective data source in autonomous driving. One of the common ways is to directly operate on the raw LiDAR point clouds [22–24, 26, 40, 41]. And another is based on transforming the point clouds onto a regular space, such as 3D voxels [45], range views [9, 28], or

pillars [14, 34, 42]. However, the measurable range of LiDAR is relatively narrow and sparse, limiting the observation of distant objects. In contrast, camera images possess a greater range and relatively dense information. This has led to the emergence of camera-only detection methods. Analogous to 2D detection methods, early methods usually predict the 3D bounding boxes based on the 2D bounding boxes [2, 20, 27, 37, 44]. Recent works further develop the direct way based on the 2D advanced detectors. FCOS3D [32] adapts a 2D-guided multi-level 3D detection and directly predicts 3D bounding boxes for each object based on FCOS [29]. Following Deformable-DETR [46], DETR3D [35] samples the corresponding features by warping learnable 3D queries in 2D images for end-to-end 3D bounding box prediction without NMS post-processing. Since the camera view is like frustum, which isn’t conducive to observation in the world coordinate system, various methods [25, 33] use a bird’s-eye view (BEV) 2D space transformation to unify the construction of information from the image in each camera view. Inspired by Lift-Splat-Shoot (LSS) [21], many methods [12, 36] further refine the transform referring to the supervision on improved depth estimation.

Multi-sensor. Both LiDAR and camera have their own advantages as mentioned above, so people started to explore the unification of the two modalities, and a lot of work has proven this to be reasonable and powerful. We categorize the existing fusion method into several forms, parallel fusion, serial fusion, and others. The Parallel fusion methods represent the work of BEVfusion [17], UVTR [15], which feeds image features into the depth estimation network to obtain pseudo-point cloud features and concatenate them with point cloud features to obtain BEV and fed into the detection head to localize the object. As for serial fusion, there is usually a semantic prior used to finding the basic association between LiDAR and image in advance. Point-Painting [30] adopts the result of semantic segmentation as the prior as well as FusionPainting [38]. The proposals of bounding boxes have also been utilized by early methods [5, 13]. However, because calibration matrices have formed a rigid link between points and pixels, such approaches are easily impacted by sensor misalignment. TransFusion [1] proposed a more effective proposal-based pipeline instead of the previous simple point-wise concatenation, enriching the contextual relationships between two modalities. Others like FUTR3D [6], achieve an end-to-end multi-modality 3D prediction by directly fusing all modality features following DETR3D [35]. In our work, we explore a novel multi-modal fusion strategy to improve the robustness and performance of 3D detection from the perspective of mutual complementation between modalities.

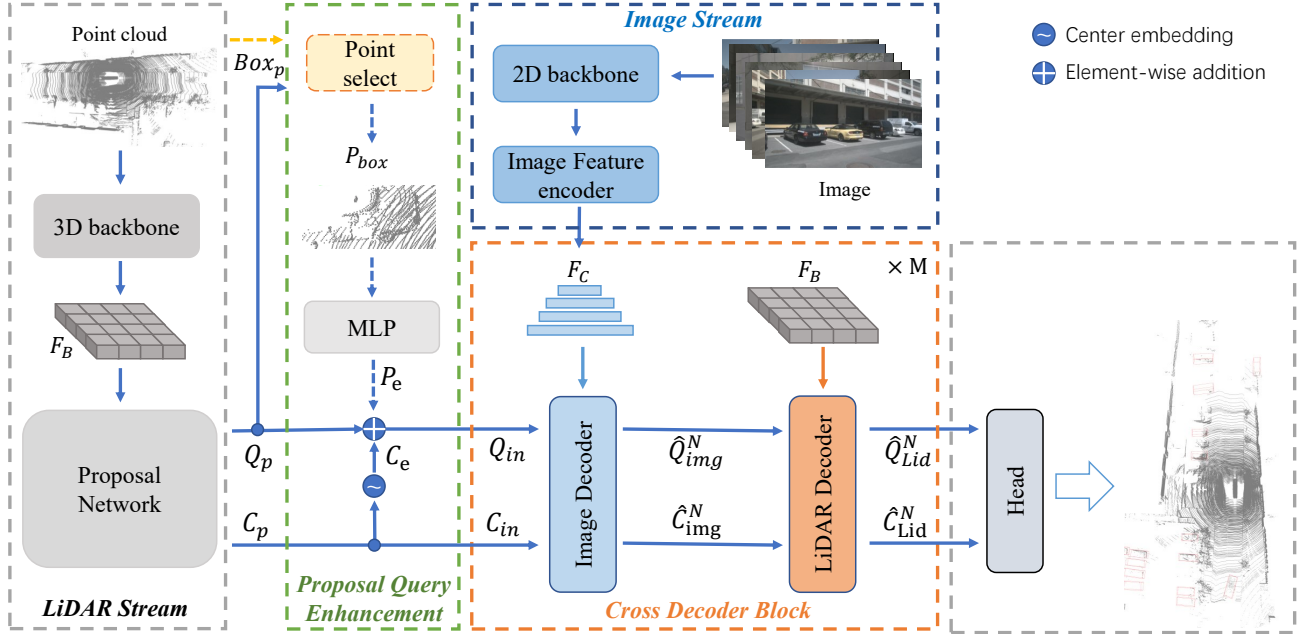


Figure 2. Overall pipeline of CrossFusion. Our model includes two main stages, and the first stage consists of the commonly used 3D backbone and proposal network, which is used to generate a set of proposal queries and the corresponding proposal centers. The second stage introduces a cross-decoder that will alternately fuse multi-scale image features and BEV features to fine-tune the result of the proposal in the first stage.

3. Methods

In this section, we present our proposed method CrossFusion for 3D object detection. As shown in Fig. 2, given the LiDAR point clouds and the corresponding multi-view camera images as inputs, CrossFusion first extracts the LiDAR BEV features F_L and multi-scale camera feature F_C from their backbones in two modal streams, respectively. Then the proposal network generates the proposals of bounding boxes and selects point clouds in the box proposals for proposal query enhancement. Finally, we introduce the cross-decoder blocks to refine the bounding boxes of objects by alternately aggregating the encoded features from the modality bridge encoder and LiDAR BEV features. Each component will be introduced in the following subsections in detail.

3.1. Image Feature Encoder

Despite acquiring the high-level features of two modalities from their respective backbone, there is a certain gap between the image features and LiDAR BEV features. Different from the previous LiDAR-Camera fusion strategy that directly fuses two features [1,6], we establish an image-view feature encoder before passing the image feature into the subsequent fusion to enrich the image semantic in the common space and bridge the modal gap.

Specifically, we use the feature maps from the back-

bone in the image stream with resolutions $\frac{1}{32}$, $\frac{1}{16}$, and $\frac{1}{8}$ of the size of the original images. Following [46], we add positional embedding and scale-level embedding to the multi-scale feature and adopt the deformable attention to enhance the feature further. We denote the output as $F_C^l \in \mathbb{R}^{d_C \times H_C^l \times W_C^l}$, where l is the number of feature levels and $H_C \times W_C$ is the size of feature map and d_C means the dimension of feature.

3.2. Proposal Query Enhancement

The query initialization in the Transformer architecture not only accelerates the training process but also improves the model accuracy, according to many excellent works for 2D detection [19,46]. Referring to this, as illustrated in Fig. 2, we design two query enhancement strategies to strengthen the representation of query for later decoding. And before that, following [1], we first adopt the input-dependent initialization to get the object queries $Q_p \in \mathbb{R}^{N \times d}$ from the proposal network, where N is the number of the proposal and d is the dimension of the whole model.

Point Selective Augmentation. Although the initial queries are favorable to improve the model training, as a double-edged sword, it can also bring over-reliance on the prior as well as the reluctance to focus on hard targets. In order to enhance the sensitivity to hard targets and reduce the over-dependence on the results of proposals, we propose a query augmentation strategy only during training,

named Point Select Enhancement. Its main insight is to add a learnable but controllable bias to the queries, forcing our model to learn the similarity to the proposal boxes rather than to chase the consistency, thereby improving the model’s robustness. Specifically, given the proposal bounding boxes Box_p predicted by Q_p , we first select Z random points $P_{rand} \in \mathbb{R}^{Z \times N \times d_{pc}}$ for an interval of candidates, where d_{pc} is the dimension of the point cloud. Then we can get the point selective embedding $P_{box} \in \mathbb{R}^{Z \times N \times d}$ via the bias projection f_{bp} , which is a Multilayer Perceptron (MLP) with the dimension of d . Finally, we will use max pooling to acquire the local optimal response $P_e \in \mathbb{R}^{N \times d}$. The formulations are as follows:

$$P_{box} = f_{bp}(P_{rand}) \quad (1)$$

$$P_e = MaxPool(P_{box}) \quad (2)$$

Proposal Center Embedding. Unlike the position information of the query is fixedly encoded or learnably parameterized [4, 46], we compensate it with the center-point prediction of the initial query. This way, the query is equipped with a prior position for better observation of the object. Specifically, we embed the 3D center point $C_{in} \in \mathbb{R}^{N \times 3}$ by a d -dimensional MLP and add the proposal center embedding $C_e \in \mathbb{R}^{N \times d}$ to Q_p .

On the whole, the input query is formulated below with the element-wise addition:

$$Q_{in}^0 = Q_p + P_e + C_e \quad (3)$$

where “0” means the original input cross decoder blocks.

3.3. Cross Decoder Block

Different from the previous fusion approaches that combine the individual features separately [1] or directly merge multi-modal features into a space [6, 17], our core idea is to take advantage of the respective modal strengths and to update the detection results through interactive decoding. Precisely, 2D images have the advantage of high recall from a wide range, and 3D point clouds have the advantage of precision from accurate geometric coordinates. To carry forward it, we stack multiple cross-decoder blocks for interleaving cross-modal fusion. To be specific, we alternated with an image decoder and a LiDAR decoder, which enables the models to alleviate the gap between the point cloud and image features and aggregate the key features between multi-modal features adaptively. In particular, the blocks built by image-LiDAR cross-decoders will increase the recall of objects located in sparse point clouds and use LiDAR-decoder to correct for these additional targets. Below are the detailed analysis and formulation of the proposed block.

Cross-modal Decoding Analysis. Many works have shown the necessity of image features at the decoding stage

[1, 15, 17], but those works may not have focused well on the specific binding order. We discover it’s some inappropriate to directly combine the image feature with the bounding box proposals previously obtained from point clouds. Concretely speaking, a single frame of the 2D image can only provide relative position information among objects and cannot acquire their absolute depths, while point clouds are capable to provide accurate 3D spatial information. This poses a problem in that the information obtained only from the camera space will lead to a relatively large bias if directly optimizing the previous proposal representations. In other words, most of the previous fundamental information underlying LiDAR space turns out to be overwhelmed. To mitigate this, we still require the LiDAR information to solidify the optimization process.

Image Decoder. Attention mechanism has been widely used in 3D detection tasks as a popular way of multi-modal information interaction [6, 17]. Here we set the image decoder layer similar to the design of Deformable DETR [46]. We use the set of N input queries $Q_{in} \in \mathbb{R}^{N \times d}$ and the corresponding proposal bounding box centers $C_{in} \in \mathbb{R}^{N \times 3}$. First, we project every center (x_i, y_i, z_i) in C_{in} into the camera coordinate system by using the calibration matrices as 2D points (u_i, v_i) in projected 2D views like Eq. (4).

$$\alpha \begin{bmatrix} u_i \\ v_i \\ 1 \end{bmatrix} = \begin{bmatrix} f_x & 0 & u_0 \\ 0 & f_y & v_0 \\ 0 & 0 & 1 \end{bmatrix} \begin{bmatrix} x_i \\ y_i \\ z_i \end{bmatrix} \quad (4)$$

where f_x, f_y, u_0, v_0 are camera intrinsic parameters, α is the scale factor. After that, we regard these 2D points as the reference points of the query set Q_{in} and sample the features from the projected views around these reference points. Eventually, we perform a weighted sum of the sampled features as the output of image-level cross-attention. Formally, let F_C be the input multi-scale image feature maps and the 2D reference points $r_C \in [0, 1]$ be normalized by the shape of the image feature maps. For each query, we update query in each cross decoder block B_m as:

$$Q_u^m = \sum_{p=1}^P \mathbf{W}_p \sum_{l=1}^L \mathbf{W}_l \left[\sum_{k=1}^K A_{lkp} \mathbf{F}_C^l(r_C + \Delta x_{lkp}) \right] \quad (5)$$

$$\hat{Q}_{img}^m = Q_u^m + Q_{img}^m \quad (6)$$

where $m \in \{1, 2, \dots, M\}$, M is the number of blocks. And k is the index of the sampling point, Δx_{lkp} and A_{lkp} denote the sampling offset and the attention weight of the k -th sampling point in l -th feature level and p -th camera, bilinear interpolation $\mathbf{F}_C^l(r_C + \Delta x_{lkp})$ is applied as in computing.

LiDAR Decoder. The structure of this decoder resembles the image decoder above. We use the query \hat{Q}_{img}^m and box center \hat{C}_p^m output from the image decoder as the input to the

LiDAR decoder. Next, we warp the box center into the BEV feature as the LiDAR-space reference point r_l and sample the BEV Feature for updating.

$$\hat{Q}_{LiD}^m = \sum_{k=1}^K A_k \mathbf{F}_L(r_L + \Delta x_k) + \hat{Q}_{img}^m \quad (7)$$

where k is the index of the sampling point, Δx_k and A_k denote the sampling offset and the attention weight of the k th sampling point, bilinear interpolation is applied as in computing $\mathbf{F}_L(r_L + \Delta x_k)$. It is worth noting that in the autonomous driving scenario, unlike images, targets on BEV are usually in the form of small objects, so we only selected the largest scale BEV feature maps to participate in the calculation.

Iterative 3D Bounding Box Refinement. Previous work has demonstrated that the iterative refinement is an effective form of improving detection performance [35,46]. Thus, we establish a similar iterative update mechanism between the image decoder and LiDAR decoder of every cross-decoder block. Specifically, we first send the query output from the image decoder to the regression branches $f_{reg,img}$ and continue to apply the offset prediction to update the bounding box center in the LiDAR decoder with its branches $f_{reg,LiD}$. The formulation is as follows:

$$\hat{C}_s^m = C_{in}^m + f_{reg,s}(\hat{Q}_s^m) \quad (8)$$

where s denotes the specific modality $\in \{img, LiD\}$. Here, each decoder block B_m refines the prediction results of the previous cross-decoder block B_{m-1} .

$$\hat{Q}_{in}^m = \hat{Q}_{LiD}^m + \hat{Q}_{in}^{m-1} \quad (9)$$

$$\hat{C}_{in}^m = \hat{C}_{LiD}^m + \hat{C}_{in}^{m-1} \quad (10)$$

where \hat{Q}_{in}^0 and \hat{C}_{in}^0 represent the output proposal query like Eq.(3) and proposal box center of the proposal network respectively.

3.4. Label Assignment and Losses

Following [4], we solve the dichotomous matching problem of prediction result and ground truth by the Hungarian algorithm. We define matching cost as the weighted sum of classification cost, regression cost, and 3D IoU cost:

$$Cost = \xi_1 L_{cls}(p, \hat{p}) + \xi_2 L_{reg}(b, \hat{b}) + \xi_3 L_{IoU}(b, \hat{b}) \quad (11)$$

where L_{cls} is the focal loss [18], L_{reg} is the L1 loss between the predicted BEV centers, scale, angle, velocity, and the ground truth, and L_{IoU} is the IoU loss [43] between the predicted boxes and ground truth boxes. ξ_1, ξ_2, ξ_3 are the coefficients of the individual cost terms. Then, we compute both the regression loss and the classification loss given the bipartite matching.

4. Implementation Details

Our implementation is based on the open-source code MMDetection3D [8]. We use VoxelNet [45] as the 3D backbone and set voxel size to (0.075m, 0.075m, 0.2m) and the detection range to $[-54m, 54m]$ for \mathbb{X} and \mathbb{Y} axis and $[-5m, 3m]$ for \mathbb{Z} axis. For the image backbone, we use ResNet-50 [11] and Dual-Swin-Tiny [16], both initialized from the instance segmentation model Mask R-CNN [10] pre-trained on nuImage [3]. We set the full-resolution image size to 896×1600 . To be friendly with memory and computational consumption, we freeze the weights of the image backbone during training. We set the $N = 400$, $Z = 25$, $M = 3$, $K_{img} = 6$ and $K_{LiD} = 1$ for training and testing. In the next experiments, we use ResNet-50 as the 2D backbone by default to align the baseline.

The data augmentation strategies and training schedules are the same as TransFusion [1]. we use random rotation with a range of $\theta \in [-\pi/4, \pi/4]$, random box scaling with a factor of $f \in [0.9, 1.1]$, random horizontal flipping in point cloud and images. furthermore, randomly reducing the resolution of LiDAR is set during training. Our training is divided into two stages: Transfusion-L [1] is chosen as our proposal network, and we first train the LiDAR stream for 20 epochs. Secondly, we keep its weights frozen in the second stage and train the cross-decoder block for 12 epochs with the batch size of 16 using 8 NVIDIA Tesla A100 GPUs. We use Adam optimizer with a one-cycle learning rate schedule, with base learning rate 1×10^{-4} , weight decay 0.01, and momentum 0.85 to 0.95. It is worth noting that we did not use the depth estimation model during training and did not use Test-Time Augmentation (TTA) or model assembly during inference.

5. Experiments

In this section, we first compare state-of-the-art methods on nuScenes. Then we designed three experiments with LiDAR corruption to show the modal complementarity of CrossFusion at low-quality LiDAR features. Afterward, we conduct extensive ablation experiments to demonstrate the rationality and importance of each key component of our CrossFusion.

nuScenes Dataset. The nuScenes dataset [3] is a large-scale autonomous-driving dataset with 3D object annotations that contains 1000 driving sequences, with 700, 150, and 150 sequences for training, validation, and testing, respectively. Each sequence is approximately 20-second long but only provides box annotations every ten frames (0.5s). Each frame contains a wealth of sensor information, including point clouds and carefully calibrated six 360-degree horizontal FOV images at the same timestamp. For 3D detection task, the main metrics are mean Average Precision (mAP) and nuScenes detection score (NDS). The

Method	Mod.	mAP	NDS	Car	Truck	C.V.	Bus	T.L.	B.R.	M.T.	Bike	Ped.	T.C.
FUTR3D [6]	LC	64.2	68.0	86.3	61.5	26.0	71.9	42.1	64.4	73.6	63.3	82.6	70.1
BEVFusion-SwinT [17] †	LC	67.9	71.0	88.6	65.0	28.1	75.4	41.4	72.2	76.7	65.8	88.7	76.9
TransFusion [1]	LC	67.3	71.2	87.6	62.0	27.4	75.7	42.8	73.9	75.4	63.1	87.8	77.0
CrossFusion	LC	69.0	71.6	88.3	66.5	32.8	75.6	43.8	70.3	77.6	67.5	89.0	78.7
CrossFusion-SwinT	LC	69.7	71.9	88.6	67.6	33.5	76.1	44.6	71.2	77.9	68.5	89.2	79.2
TransFusion-L [1]	L	65.5	70.2	86.2	56.7	28.2	66.3	58.8	78.2	68.3	44.2	86.1	82.0
PointAugmenting [31]	LC	66.8	71.0	87.5	57.3	28.0	65.2	60.7	72.6	74.3	50.9	87.9	83.6
FusionPainting [38]	LC	68.1	71.6	87.1	60.8	30.0	68.5	61.7	71.8	74.7	53.5	88.3	85.0
TransFusion [1]	LC	68.9	71.7	87.1	60.0	33.1	68.3	60.8	78.1	73.6	52.9	88.4	86.7
BEVFusion-SwinT [17] †	LC	69.2	71.8	88.1	60.9	34.4	69.3	62.1	78.2	72.2	52.2	89.2	85.2
CrossFusion	LC	69.2	71.8	87.4	60.4	33.8	70.3	61.0	74.3	74.3	56.1	89.2	85.1
CrossFusion-SwinT	LC	70.1	72.2	87.7	62.4	34.7	71.5	61.8	75.0	75.1	57.5	89.6	85.1

Table 1. Comparison with state-of-the-art methods on nuScenes validation (top) and test (bottom) set. Metrics: mAP(%), NDS (%), and AP (%) for each category. ‘C.V.’, ‘T.L.’, ‘B.R.’, ‘M.T.’, ‘Ped.’, and ‘T.C.’ are short for construction vehicle, trailer, barrier, motor, pedestrian, and traffic cone, respectively. ‘L’ and ‘C’ represent LiDAR and the camera, respectively. We highlight the best performances across all methods with **bold**. †means use depth estimation pre-trained network.

mAP defines a match by considering the 2D center distance thresholds of $0.5m, 1m, 2m, 4m$ across ten classes on the ground plane. NDS is a weighted average of mAP and other attribute metrics, including translation(mATE), scale(mASE), orientation(mAOE), velocity(mAVE), and attribute(mAAE).

5.1. Main Results

We compare the results of our CrossFusion on the nuScenes validation set and test set with the state-of-the-art methods. As shown in Tab. 1, without model ensemble and depth estimation pre-trained network, our approach surpasses all existing LiDAR-camera fusion methods in both the validation set and test set. our model achieves 69.7% mAP and 71.9% NDS in the validation set and 70.1% mAP and 72.2% NDS in the test set, respectively. The results show that we can exceed the results of TransFusion on both the validation set(+2.4% mAP) and the test set(+0.3% mAP). The nuScenes leaderboard shows that methods with depth priors typically carry more powerful multi-modal modeling capabilities. For a fair comparison, we replace 2D backbone with Dual-Swin-Tiny [16], and we find that CrossFusion can outperform the competitor with depth estimation pre-training, BEVFusion. Meanwhile, our performance has improved in most classes, especially in two small categories, motor, and bike, with mAP improvements of 2.9% and 3.3%, respectively. We ascribe the performance improvement to further exploration of the multi-modal perception capability via our interleaving fusion strategy.

5.2. Robustness against Low-quality LiDAR

We designed three different experiments with missing point clouds to simulate possible LiDAR malfunctions in autonomous driving scenarios. Experiments show

that CrossFusion can exhibit strong robustness without re-training for specific scenarios. To avoid overstatement, We choose Transfusion, a well-known robust model on the nuScenes dataset, as our baseline for comparing the robustness of our method.

Randomly LiDAR Beams Data Augmentation. To improve the robustness of the model, we propose an effective data enhancement strategy. Inspired by FUTR [6], we try to train the network using LiDAR with different resolutions. Following FUTR, we simulated two low-resolution LiDAR beams with 16-beam and 4-beam from the original nuScenes 32-beam LiDAR point clouds. In detail, we first convert the point cloud in the Cartesian coordinate system to the spherical coordinate system, then we select the inclination angle in $[-30^\circ, 10^\circ]$ as 4-beam LiDAR. The inclination range of the 16-beam LiDAR is $[-7.1^\circ, -5.8^\circ] \cup [-4.5^\circ, -3.2^\circ] \cup [-1.9^\circ, -0.6^\circ] \cup [0.7^\circ, 2.0^\circ]$. Data augmentation takes effect after every 10 iterations during training, and we randomly select a low-resolution LiDAR as input. In the following, we use **CrossFusion*** to indicate that the data augmentation is used.

Low-resolution LiDAR. LiDAR is highly susceptible to dust or water droplets suspended in the air. For example, in common rainy and foggy weather, LiDAR may not be able to receive the signal reflected by the object due to signal attenuation, which may lead to the problem of reduced resolution. As shown in Tab. 2, when we used the data augmentation method mentioned above to obtain 16-beam and 4-beam LiDAR point clouds as input, CrossFusion showed a strong ability to resist LiDAR feature degeneration. When the number of beams of LiDAR is reduced to 16, our method improves by 3.8% mAP and 1.8% NDS compared to TransFusion. Surprisingly when the input is 4-beam, our model has a 3.6% mAP and 1.4% NDS improve-

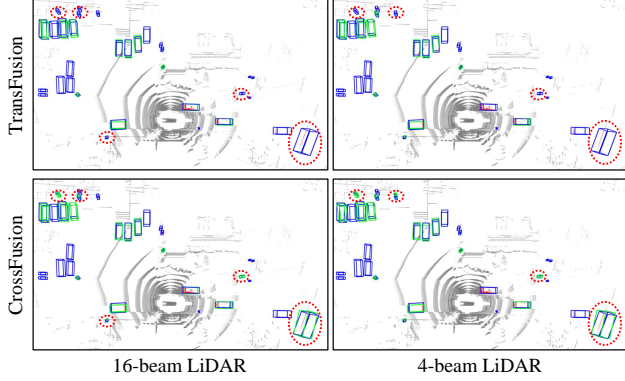


Figure 3. Results on robustness setting of Low-resolution LiDAR. The red dashed circles represent more recall of our method compared to TransFusion. Blue boxes and green boxes are the ground truth and predictions, respectively. Best viewed with color and zoom-in.

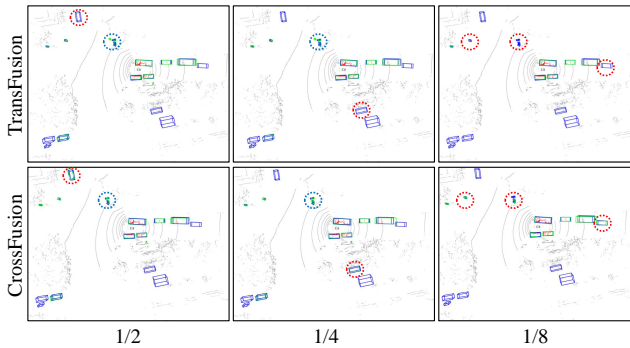


Figure 4. Results on robustness setting of reduced points. The red dashed circles represent more recall of our method compared to TransFusion, and the blue dashed circles represent error detection. Blue boxes and green boxes are the ground truth and predictions, respectively. Best viewed with color and zoom-in.

ment compared to Transfusion, even without data augmentation. If we enable data augmentation, the gain of mAP and NDS will be increased to 5.2% and 2.4%, respectively. We speculate that the performance enhancement is because the interleaving fusion strategy helps to exploit modal complementarity. The results reveal that randomly LiDAR beams augmentation can drive the model to mine more connections between image features and LiDAR features for better robustness. As can be seen from the visualization in Fig. 3, we can obtain more recall with low-resolution LiDAR input, especially in the challenging pedestrian category, which may better guarantee the safety of autonomous driving. In addition, low-resolution LiDAR is usually more affordable, and our model exhibits the possibility of deploying at a low cost.

Reduced Number Of Points. LiDAR is susceptible to surrounding light and vulnerable to the reflection rate of ob-

jects. The point cloud is easily lost in outdoor environments when exposed to bright light or highly reflective materials. Tab. 3 presents the results of reducing the points to half, a quarter, and an eighth of the original points, respectively. It is proof that CrossFusion has better results for all reduction ratios, and the advantage of our method becomes more obvious the larger the reduction ratio is. Noteworthy, when the points are only one-eighth of the original points, CrossFusion can increase mAP and NDS by 4.6% and 2.5%, respectively, compared to Transfusion. This demonstrates that CrossFusion is less dependent on LiDAR features and has the potential for modal complementarity. As shown in the Fig. 4, our method can compensate for the deficiencies of LiDAR target point clouds to a certain extent. When reduced to a quarter of the point cloud, as shown in the blue dashed circles, Transfusion has false detections due to missing point cloud features, while our model can still show satisfactory detection results.

Method	Beam	mAP	NDS
TransFusion [1]	16	51.5	61.8
CrossFusion		54.8(+3.3)	63.3(+1.5)
CrossFusion*		55.3(+3.8)	63.6(+1.8)
TransFusion [1]	4	39.2	54.3
CrossFusion		42.8(+3.6)	55.9(+1.4)
CrossFusion*		44.4(+5.2)	56.7(+2.4)

Table 2. Low-resolution LiDAR simulated on the nuScenes validation dataset as input for mAP and NDS. Beam settings are the same as Randomly LiDAR Beams Data Augmentation. The numbers in parentheses represent the improvement compared to the baseline.

Method	Ratio	mAP	NDS
TransFusion [1]	1/2	63.8	68.5
CrossFusion		66.1(+2.3)	69.6(+0.3)
CrossFusion*		66.1(+2.3)	69.6(+0.3)
TransFusion [1]	1/4	56.4	63.7
CrossFusion		59.3(+1.9)	65.2(+1.5)
CrossFusion*		59.7(+2.3)	65.4(+1.7)
TransFusion [1]	1/8	44.6	55.8
CrossFusion		48.4(+3.8)	57.8(+2.0)
CrossFusion*		49.2(+4.6)	58.3(+2.5)

Table 3. Random reduction of points results in the nuScenes validation dataset. “Ratio” indicates the ratio of the input points to the original points after random reduction.

Reduced LiDAR Field Of View. The most vulnerable part of the spinning LiDAR is the rotating mechanism, and it will bring the problem of missing Field of view (FOV). To simulate the above situation, we adjusted the FOV of the LiDAR, and the results are shown in Tab. 4. Experimental re-

sults show that our method has mAP and NDS gain at each set compared to the baseline. This demonstrates that CrossFusion is more robust, and our fusion method has a certain compensation effect on the reduction of LiDAR FOV.

Method	FOV	mAP	NDS
TransFusion [1]		50.1	62.2
CrossFusion	$-\frac{5\pi}{6}, \frac{5\pi}{6}$	51.6(+1.5)	62.8(+0.6)
CrossFusion*		51.8(+1.7)	62.9(+0.7)
TransFusion [1]		38.7	56.4
CrossFusion	$-\frac{2\pi}{3}, \frac{2\pi}{3}$	40.0(+1.3)	56.9(+0.5)
CrossFusion*		40.1(+1.4)	56.9(+0.5)
TransFusion [1]		29.6	51.6
CrossFusion	$-\frac{\pi}{2}, \frac{\pi}{2}$	30.6(+1.0)	52.0(+0.4)
CrossFusion*		30.7(+1.1)	52.0(+0.4)
TransFusion [1]		20.5	46.4
CrossFusion	$-\frac{\pi}{3}, \frac{\pi}{3}$	21.1(+0.6)	46.5(+0.1)
CrossFusion*		21.2(+0.7)	46.6(+0.2)

Table 4. Compare the results of CrossFusion at different FOVs on the nuScenes validation set. Numbers in parentheses represent an improvement over the baseline.

Idx	CDB	IFE	PSE	mAP	NDS
a)	-	-	-	65.2	69.9
b)	✓	-	-	67.9	71.1
c)	✓	✓	-	67.9	71.2
d)	✓	-	✓	68.0	70.9
e)	✓	✓	✓	68.5	71.3

Table 5. Ablation of our key component. ‘‘CDB’’ and ‘‘IFE’’ means Cross Decoder Block and Image Feature Encoder, respectively, and ‘‘PSE’’ represents Point Select Enhancement.

5.3. Ablation Studies

To demonstrate the effectiveness of each component of CrossFusion, we performed an ablation study of them on the nuScenes validation set. For fast iteration, we train 8 epochs by default.

Ablation of key components. As shown in Tab. 5, the first line indicates the result of the proposal network. **b)** When the cross-decoder block is added, mAP and NDS can be improved by 2.7% and 1.2%, respectively. This shows that the strategy of using interleaving fusion, which is able to interact with image features and BEV features, provides richer instance-level features, gaining 2.7% mAP and 1.2% NDS. **c)** NDS 0.1% gain when the image feature encoder is added separately. This is because Cross decoder block has fully interacted with the instance features and point cloud features of the image. Adding more image features will only continue to optimize the bounding box that is already close to the ground truth. **d)** When point select enhancement is

added, the network will be more sensitive to learning difficult samples, bringing 0.1% mAP gain and leading to the loss of bounding box accuracy. **e)** With the combination of the above two modules, the mAP is improved by 0.6% compared to **b)**. This shows that with the help of point select enhancement, higher-quality image information needs to be introduced to effectively help learn hard samples.

Number Of Fusion Components. As shown in Tab. 6, a two-layer image feature encoder is appropriate. Adding more encoders may lead to overfitting and thus affect performance. In Tab. 7, increasing the number of cross-decoder blocks to three allows for continuous performance growth. So we choose this parameter in our model to achieve the best results.

L_{IFE}	mAP	NDS	mATE	mASE	mAOE
1	68.5	71.3	28.3	25.8	29.6
2	68.8	71.4	28.5	25.8	29.2
3	68.3	71.1	28.4	26.2	28.9

Table 6. Performance among different encoder layers, L_{IFE} represents the number of layers of the image feature encoder.

L_{CDB}	mAP	NDS	mATE	mASE	mAOE
2	68.2	71.2	28.4	25.6	29.2
3	68.8	71.4	28.5	25.8	29.2
4	68.4	71.0	28.6	26.4	29.5

Table 7. The impact of the number of cross decoder blocks on performance, L_{CDB} represents the number of cross decoder blocks.

Idx	Order	mAP	NDS	mATE	mASE	mAOE
a)	(LC)3	65.5	69.2	28.9	25.3	30.9
b)	3L3C	65.5	69.4	28.9	25.7	30.1
c)	3C3L	67.8	71.0	28.4	25.8	28.8
d)	(CL)3	68.5	71.3	28.3	25.8	29.6

Table 8. The ablation of the decoding order inside the cross-decoder block.

The Order Of Decoding. We designed four different decoding orders to explore the impact of different decoder arrangements on CrossFusion performance. For the convenience of representation, we will write the LiDAR decoder as ‘‘L’’ and the image decoder as ‘‘C’’. Thus our setting can be denoted by ‘‘(CL) 3’’, which means 3-layer combination consisting of first ‘‘C’’ and then ‘‘L’’. Analogously, ‘‘3L3C’’ means in series of first 3 layers of ‘‘L’’ then 3 layers of ‘‘C’’. Below are other combinations we select, which are (LC)3 and 3L3C. The Tab. 8 shows that the performance of both **a)** and **b)** is lower than that of **c)** and **d)**. We speculate it is

not reasonable to try to update the LiDAR proposal with accurate 3D information using image features without depth information. Under the premise of determining a reasonable order, **d**), **e**) the interleaving fusion strategy outperforms the serial fusion approach by 0.7% mAP. The experimental results show that the decoder architecture with interleaving fusion can make the model have stronger multi-modal modeling capability.

6. Conclusion

In this paper, we propose CrossFusion, a novel LiDAR-camera fusion framework without depth pre-training. We design the interleaving fusion strategies with multi-level proposal query enhancements to pursue equilibrium and complementarity between modalities. Extensive experiments have demonstrated the robustness and noise-resistance of our model, which better mines image information to combat LiDAR corruption. We hope that our work will stimulate further exploration of robust multi-modal fusion in autonomous driving scenarios.

References

- [1] Xuyang Bai, Zeyu Hu, Xinge Zhu, Qingqiu Huang, Yilun Chen, Hongbo Fu, and Chiew-Lan Tai. Transfusion: Robust lidar-camera fusion for 3d object detection with transformers. In *IEEE Conf. Comput. Vis. Pattern Recog.*, pages 1090–1099, 2022. [1](#), [2](#), [3](#), [4](#), [5](#), [6](#), [7](#), [8](#)
- [2] Garrick Brazil and Xiaoming Liu. M3d-rpn: Monocular 3d region proposal network for object detection. In *Proceedings of the IEEE/CVF International Conference on Computer Vision*, pages 9287–9296, 2019. [2](#)
- [3] Holger Caesar, Varun Bankiti, Alex H Lang, Sourabh Vora, Venice Erin Liong, Qiang Xu, Anush Krishnan, Yu Pan, Giancarlo Baldan, and Oscar Beijbom. nuscenes: A multi-modal dataset for autonomous driving. In *Proceedings of the IEEE/CVF conference on computer vision and pattern recognition*, pages 11621–11631, 2020. [1](#), [5](#)
- [4] Nicolas Carion, Francisco Massa, Gabriel Synnaeve, Nicolas Usunier, Alexander Kirillov, and Sergey Zagoruyko. End-to-end object detection with transformers. In *European conference on computer vision*, pages 213–229. Springer, 2020. [4](#), [5](#)
- [5] Xiaozhi Chen, Huimin Ma, Ji Wan, Bo Li, and Tian Xia. Multi-view 3d object detection network for autonomous driving. *2017 IEEE Conference on Computer Vision and Pattern Recognition (CVPR)*, pages 6526–6534, 2017. [1](#), [2](#)
- [6] Xuanyao Chen, Tianyuan Zhang, Yue Wang, Yilun Wang, and Hang Zhao. Futr3d: A unified sensor fusion framework for 3d detection. *arXiv preprint arXiv:2203.10642*, 2022. [1](#), [2](#), [3](#), [4](#), [6](#)
- [7] Yukang Chen, Jianhui Liu, Xiaojuan Qi, Xiangyu Zhang, Jian Sun, and Jiaya Jia. Scaling up kernels in 3d cnns. *arXiv preprint arXiv:2206.10555*, 2022. [1](#)
- [8] MMDetection3D Contributors. MMDetection3D: OpenMMLab next-generation platform for general 3D object detection. <https://github.com/open-mmlab/mmdetection3d>, 2020. [5](#)
- [9] Lue Fan, Xuan Xiong, Feng Wang, Naiyan Wang, and Zhaoxiang Zhang. Rangedet: In defense of range view for lidar-based 3d object detection. In *Proceedings of the IEEE/CVF International Conference on Computer Vision*, pages 2918–2927, 2021. [2](#)
- [10] Kaiming He, Georgia Gkioxari, Piotr Dollár, and Ross Girshick. Mask r-cnn. In *Proceedings of the IEEE international conference on computer vision*, pages 2961–2969, 2017. [5](#)
- [11] Kaiming He, Xiangyu Zhang, Shaoqing Ren, and Jian Sun. Deep residual learning for image recognition. In *Proceedings of the IEEE conference on computer vision and pattern recognition*, pages 770–778, 2016. [5](#)
- [12] Junjie Huang, Guan Huang, Zheng Zhu, and Dalong Du. Bevdet: High-performance multi-camera 3d object detection in bird-eye-view. *arXiv preprint arXiv:2112.11790*, 2021. [2](#)
- [13] Jason Ku, Melissa Mozifian, Jungwook Lee, Ali Harakeh, and Steven L. Waslander. Joint 3d proposal generation and object detection from view aggregation. *2018 IEEE/RSJ International Conference on Intelligent Robots and Systems (IROS)*, pages 1–8, 2018. [1](#), [2](#)
- [14] Alex H Lang, Sourabh Vora, Holger Caesar, Lubing Zhou, Jiong Yang, and Oscar Beijbom. Pointpillars: Fast encoders for object detection from point clouds. In *Proceedings of the IEEE/CVF conference on computer vision and pattern recognition*, pages 12697–12705, 2019. [2](#)
- [15] Yanwei Li, Yilun Chen, Xiaojuan Qi, Zeming Li, Jian Sun, and Jiaya Jia. Unifying voxel-based representation with transformer for 3d object detection. In *Adv. Neural Inform. Process. Syst.*, 2022. [1](#), [2](#), [4](#)
- [16] Tingting Liang, Xiaojie Chu, Yudong Liu, Yongtao Wang, Zhi Tang, Wei Chu, Jingdong Chen, and Haibin Ling. Cbnet: A composite backbone network architecture for object detection. *IEEE Transactions on Image Processing*, 2022. [5](#), [6](#)
- [17] Tingting Liang, Hongwei Xie, Kaicheng Yu, Zhongyu Xia, Zhiwei Lin, Yongtao Wang, Tao Tang, Bing Wang, and Zhi Tang. BEVFusion: A Simple and Robust LiDAR-Camera Fusion Framework. In *Adv. Neural Inform. Process. Syst.*, 2022. [1](#), [2](#), [4](#), [6](#)
- [18] Tsung-Yi Lin, Priya Goyal, Ross Girshick, Kaiming He, and Piotr Dollár. Focal loss for dense object detection. In *Proceedings of the IEEE international conference on computer vision*, pages 2980–2988, 2017. [5](#)
- [19] Depu Meng, Xiaokang Chen, ZeJia Fan, Gang Zeng, Houqiang Li, Yuhui Yuan, Lei Sun, and Jingdong Wang. Conditional detr for fast training convergence. In *Proceedings of the IEEE/CVF International Conference on Computer Vision*, pages 3651–3660, 2021. [3](#)
- [20] Arsalan Mousavian, Dragomir Anguelov, John Flynn, and Jana Kosecka. 3d bounding box estimation using deep learning and geometry. In *Proceedings of the IEEE conference on Computer Vision and Pattern Recognition*, pages 7074–7082, 2017. [2](#)
- [21] Jonah Philion and Sanja Fidler. Lift, splat, shoot: Encoding images from arbitrary camera rigs by implicitly unprojecting

- to 3d. In *European Conference on Computer Vision*, pages 194–210. Springer, 2020. 2
- [22] Charles R Qi, Wei Liu, Chenxia Wu, Hao Su, and Leonidas J Guibas. Frustum pointnets for 3d object detection from rgb-d data. In *Proceedings of the IEEE conference on computer vision and pattern recognition*, pages 918–927, 2018. 2
- [23] Charles R Qi, Hao Su, Kaichun Mo, and Leonidas J Guibas. Pointnet: Deep learning on point sets for 3d classification and segmentation. In *Proceedings of the IEEE conference on computer vision and pattern recognition*, pages 652–660, 2017. 2
- [24] Charles Ruizhongtai Qi, Li Yi, Hao Su, and Leonidas J Guibas. Pointnet++: Deep hierarchical feature learning on point sets in a metric space. *Advances in neural information processing systems*, 30, 2017. 2
- [25] Cody Reading, Ali Harakeh, Julia Chae, and Steven L Waslander. Categorical depth distribution network for monocular 3d object detection. In *Proceedings of the IEEE/CVF Conference on Computer Vision and Pattern Recognition*, pages 8555–8564, 2021. 2
- [26] Shaoshuai Shi, Xiaogang Wang, and Hongsheng Li. Pointcnn: 3d object proposal generation and detection from point cloud. In *Proceedings of the IEEE/CVF conference on computer vision and pattern recognition*, pages 770–779, 2019. 2
- [27] Andrea Simonelli, Samuel Rota Bulo, Lorenzo Porzi, Manuel López-Antequera, and Peter Kotschieder. Disentangling monocular 3d object detection. In *Proceedings of the IEEE/CVF International Conference on Computer Vision*, pages 1991–1999, 2019. 2
- [28] Pei Sun, Weiyue Wang, Yuning Chai, Gamaleldin Elsayed, Alex Bewley, Xiao Zhang, Cristian Sminchisescu, and Dragomir Anguelov. Rsn: Range sparse net for efficient, accurate lidar 3d object detection. In *Proceedings of the IEEE/CVF Conference on Computer Vision and Pattern Recognition*, pages 5725–5734, 2021. 2
- [29] Zhi Tian, Chunhua Shen, Hao Chen, and Tong He. Fcos: Fully convolutional one-stage object detection. In *Proceedings of the IEEE/CVF international conference on computer vision*, pages 9627–9636, 2019. 2
- [30] Sourabh Vora, Alex H. Lang, Bassam Helou, and Oscar Beijbom. Pointpainting: Sequential fusion for 3d object detection. *IEEE Conf. Comput. Vis. Pattern Recog.*, pages 4603–4611, 2020. 1, 2
- [31] Chunwei Wang, Chao Ma, Ming Zhu, and Xiaokang Yang. Pointaugmenting: Cross-modal augmentation for 3d object detection. In *Proceedings of the IEEE/CVF Conference on Computer Vision and Pattern Recognition*, pages 11794–11803, 2021. 1, 6
- [32] Tai Wang, Xinge Zhu, Jiangmiao Pang, and Dahua Lin. Fcos3d: Fully convolutional one-stage monocular 3d object detection. In *Proceedings of the IEEE/CVF International Conference on Computer Vision*, pages 913–922, 2021. 2
- [33] Yan Wang, Wei-Lun Chao, Divyansh Garg, Bharath Hariharan, Mark Campbell, and Kilian Q Weinberger. Pseudolidar from visual depth estimation: Bridging the gap in 3d object detection for autonomous driving. In *Proceedings of the IEEE/CVF Conference on Computer Vision and Pattern Recognition*, pages 8445–8453, 2019. 2
- [34] Yue Wang, Alireza Fathi, Abhijit Kundu, David A Ross, Caroline Pantofaru, Tom Funkhouser, and Justin Solomon. Pillar-based object detection for autonomous driving. In *European Conference on Computer Vision*, pages 18–34. Springer, 2020. 2
- [35] Yue Wang, Vitor Campagnolo Guizilini, Tianyuan Zhang, Yilun Wang, Hang Zhao, and Justin Solomon. Detr3d: 3d object detection from multi-view images via 3d-to-2d queries. In *Conference on Robot Learning*, pages 180–191. PMLR, 2022. 2, 5
- [36] Enze Xie, Zhiding Yu, Daquan Zhou, Jonah Philion, Anima Anandkumar, Sanja Fidler, Ping Luo, and Jose M Alvarez. M²bev: Multi-camera joint 3d detection and segmentation with unified birds-eye view representation. *arXiv preprint arXiv:2204.05088*, 2022. 2
- [37] Bin Xu and Zhenzhong Chen. Multi-level fusion based 3d object detection from monocular images. In *Proceedings of the IEEE conference on computer vision and pattern recognition*, pages 2345–2353, 2018. 2
- [38] Shaoqing Xu, Dingfu Zhou, Jin Fang, Junbo Yin, Zhou Bin, and Liangjun Zhang. Fusionpainting: Multimodal fusion with adaptive attention for 3d object detection. In *2021 IEEE International Intelligent Transportation Systems Conference (ITSC)*, pages 3047–3054. IEEE, 2021. 1, 2, 6
- [39] Yan Yan, Yuxing Mao, and Bo Li. Second: Sparsely embedded convolutional detection. *Sensors*, 18(10):3337, 2018. 1
- [40] Zetong Yang, Yanan Sun, Shu Liu, and Jiaya Jia. 3dssd: Point-based 3d single stage object detector. In *Proceedings of the IEEE/CVF conference on computer vision and pattern recognition*, pages 11040–11048, 2020. 2
- [41] Zetong Yang, Yanan Sun, Shu Liu, Xiaoyong Shen, and Jiaya Jia. Std: Sparse-to-dense 3d object detector for point cloud. In *Proceedings of the IEEE/CVF international conference on computer vision*, pages 1951–1960, 2019. 2
- [42] Tianwei Yin, Xingyi Zhou, and Philipp Krahenbuhl. Center-based 3d object detection and tracking. In *Proceedings of the IEEE/CVF conference on computer vision and pattern recognition*, pages 11784–11793, 2021. 2
- [43] Dingfu Zhou, Jin Fang, Xibin Song, Chenye Guan, Junbo Yin, Yuchao Dai, and Ruigang Yang. Iou loss for 2d/3d object detection. In *2019 International Conference on 3D Vision (3DV)*, pages 85–94. IEEE, 2019. 5
- [44] Xingyi Zhou, Dequan Wang, and Philipp Krähenbühl. Objects as points. *arXiv preprint arXiv:1904.07850*, 2019. 2
- [45] Yin Zhou and Oncel Tuzel. Voxelnet: End-to-end learning for point cloud based 3d object detection. In *IEEE Conf. Comput. Vis. Pattern Recog.*, pages 4490–4499, 2018. 1, 2, 5
- [46] Xizhou Zhu, Weijie Su, Lewei Lu, Bin Li, Xiaogang Wang, and Jifeng Dai. Deformable detr: Deformable transformers for end-to-end object detection. *arXiv preprint arXiv:2010.04159*, 2020. 2, 3, 4, 5